DEVELOPMENT OF THE DYNA3D SIMULATION CODE WITH AUTOMATED FRACTURE PROCEDURE FOR BRICK ELEMENTS

Ala Tabiei[1] and Jin Wu[2]

CENTER OF EXCELLENCE IN DYNA3D ANALYSIS
Department of Aerospace Eng. & Eng. Mechanics
University of Cincinnati, Cincinnati, OH 45221-0070
www.ase.uc.edu/~atabiei

ABSTRACT

Numerical simulation of cracked structures is an important aspect in structural safety assessment. In recent years, there has been an increasing rate of development of numerical codes for modeling fracture procedure. The subject of this investigation is implementing automated fracture models in the DYNA3D nonlinear explicit finite element code to simulate pseudo 3-D crack growth procedure. The implemented models have the capabilities of simulating automatic crack propagation without user intervention. The implementation is carried on solid elements. The methodology of implementing fracture models is described. An element deletion-and-replacement remeshing procedure is proposed for updating the explicit geometric description of evolving cracks. Fracture parameters such as stress intensity factors, energy release rates and crack tip opening angle are evaluated. The maximum circumferential stress criterion is utilized to predict the direction of crack advancement. Seven crack problems are presented to verify the effectiveness of the methodology. Mesh sensitivity and loading rate effects are studied in the validation of the presented procedure.

Keyword: pseudo 3-D fracture simulations, fracture procedures, fracture and nonlinear explicit finite element, DYNA3D.

[1] Associate Professor and Director
[2] Graduate Research Assistant

INTRODUCTION

Numerical analysis of cracked structures subjected to various kinds of actions is an important issue for structural safety. It undoubtedly aids in having a good knowledge of the possibility for an existing crack to growth. Many numerical methods have been developed for the simulation of fracture processes. Three kinds of well-known numerical models exist to discretize structures as follows:

(1) the finite element method,
(2) the boundary element method,
(3) the element-free Galerkin method.

The finite element method (FEM) has been in use for over 40 years and is now established as a powerful numerical technique for solution of partial differential equations. The field of fracture mechanics has benefited significantly by advances in finite element technology. Finite element methodology specific to the analysis of fracture mechanics problems has been reviewed by Liebowitz and Moyer (1989). The important algorithmic developments which have enhanced the numerical modeling of fracture processes were described in this literature.
The boundary element method (Aliabadi 1993; Portela 1993; and Mi 1996) is a well established technique for the numerical solution of boundary integral equations that govern the displacements of the crack faces in a cracked body. This technique avoids a large effort of the remeshing since only the line or surface representing the crack needs to be remeshed. A comprehensive review of the boundary element formulations in fracture mechanics can be found in Aliabadi (1997).

The element-free Galerkin (EFG) method was developed by Belytscho and coworkers (Belytschko 1994; Belytschko 1995; and Krysl 1999). It has been proved to offer many attractive features in the modeling of crack propagation. The element free Galerkin method utilizes the gridless method for solving partial differential equations by employing least square interpolants for the trial and test functions along with a variational principle (weak form). The approach requires only nodes and a description of the external and internal boundaries and interfaces of the model. No element connectivity is needed. In the EFG method, the domain boundary is explicitly represented, as it is in the finite element methods, and the domain itself is filled with nodes and (non-collocated) integration points. However, the displacement interpolant is constructed without reference to any explicit connectivity among the nodes. Instead, the interpolant, and its gradient, at the integration points are obtained by applying a moving-least-squares interpolation to the nodes that lie within the *domain of influence* of a given integration point. The domain of influence is normally taken to be a disc (sphere in three dimensions), with a 'line-of-sight' modification near the domain boundary: only nodes that can be reached by a straight line that does not pass through the boundary are included in the domain of influence for a given integration point. For an integration point that lies in the vicinity of an extending crack, this feature causes the set of nodes within its domain of influence to change abruptly as the crack advances. (for more details see Rashid 1998).
Although numerical difficulties still exist, the finite element method has been widely used for fracture problems. Koenke et al. (1998) presented a review of numerical techniques for the modeling of crack growth. Three basic categories were distinguished in the literature and summarized as follows:

1. Crack propagation using the smeared crack approach

This concept has been widely used in finite element simulations for the studies of failure analysis (Scordelis 1972; Argyris 1979; Lee 1982; Chang 1987; Hwang 1989; and Vaziri 1992). The method associates fracture with element stiffness loss. In this technique, the stress in each element is monitored. The failed element remains a continuum but loses its load carrying capacity (stiffness and/or strength) in certain directions. A crack is therefore not represented explicitly, but modeled as a "smeared crack" by modifying the material constitutive relations in a suitable way. The methodology is relatively simple to implement, and eliminates the meshing process from each simulation step. However, since the stresses or strains are checked at the center of the elements, these stresses or strains are smaller than those at the crack tip so that the applied stress which causes fracture is overestimated (Marzougui, 1998). Moreover, the effective loss of material at the crack tip significantly alters the crack tip geometry. Results of crack propagation simulations are also highly sensitive to the mesh size used. For materials failing in a diffuse manner, such as concrete, this method has been successfully used. However, since the crack tip in metals remains relatively distinct, the crack tip geometry can not be simulated by smeared crack approaches precisely. If elements in the region of the expected crack path become too small, there may arise a lack of convergence. Furthermore, the phenomenon of "stress-locking" can occur in the case of crack propagation not parallel to the direction of element edges. Elements in the region of the crack show artificially large stresses. The overall displacements in the model may be accurate, but stresses and strain energies calculated within finite elements will be incorrect in the crack region (Koenke et al., 1998).

2. Discrete crack propagation using the nodal release approach

The nodal release approach has been proven to be very robust and easy to implement, even in commercial FE codes, and remains a popular technique to model fracture procedure (for details see Yagawa 1977; Keegtra 1978; and Bolukbasi 1995). In this concept, two element edges, initially constrained to identical displacements, are allowed to separate by releasing the constraints and nodal forces which hold the elements together. A new free crack surface is therefore generated at the crack interface. In this technique a crack is assumed to propagate along existing edges of the element mesh. At each step, one element corner node or edge node is separated into two nodes and the crack extends along the respective element length. This approach clearly produces an explicit crack opening profile and has a great advantage of minimal effort for the mesh modification. It has been proven to be very efficient if a crack trajectory is known a priori (Rankin, 1993). But this method is greatly mesh dependence. For the problems in which the crack path is uncertain a very fine mesh with considerable numerical effort has to be applied.

3. Discrete crack propagation using the delete-and-fill remeshing method

This concept was first introduced by Saouma and Ingraffea (Wawrzynek, 1991) in the early 1980s. The approach uses the strategy of the delete-and-fill process for the modeling: First, a group of elements in a region around crack front is deleted. After the crack is extended, the local domain is refilled with new elements for the new crack tip. The method of remeshing intermittently recreates the computational model and allocates the necessary resources to the current critical regions of the model. This technique makes it possible to simulate the arbitrary curvilinear crack propagation by automatic remeshing process. Currently a number of methodologies were described in the literature to fill a 2-D arbitrary domain (Henshell 1975; Barsoum 1977; and Lee 1992). However fewer algorithms exist for the generation of 3-D arbitrary meshes. Three-dimensional crack propagation involves an evolving 3-D surface,

whereas 2-D crack growth can be represented by elongation of a line. Modeling 3-D crack growth is therefore inherently more complicated than modeling 2-D crack growth. It is still a challenging issue in the development of finite element algorithms.

Several new finite element techniques have been developed to model crack propagation without remeshing. An alternative approach to remeshing for modeling of running cracks involves the use of moving mesh technique. Atluri et al. (1980) utilized this concept in the moving singular element studies. A hybrid element was used to produce reasonable results. The main problem with the hybrid approach is the complexity of formulation and difficulty in the implementation (Liebowitz, 1995). Rashid (1998) also presented a 2-D moving mesh technique called the Arbitrary Local Mesh Replacement (ALMR) method. In his method, two distinct meshes are employed: one that surrounds the advancing crack front and moves with it, and the other that fills the entire domain. Minimal remeshing finite element method was proposed by Belytschko and Black (1999). In this approach, discontinuous enrichment functions are added to the finite element approximation to account for the presence of the 2-D crack. The crack is allowed to be arbitrarily aligned within the mesh. For severely curved cracks, remeshing may be needed but only away from the crack tip where remeshing is much easier.

Currently a considerable amount of effort has been focused on the 3-D crack growth simulations. Krysl and Belytschko (1999) provided an overview of the literature on this area. The EFG method was utilized by Krysl and Belytschko (1999) for modeling arbitrary three-dimensional dynamically propagating cracks in elastic bodies. Mi and Aliabadi (1994) presented an application of a dual boundary element method to quasi-static and fatigue 3-D crack propagation. Dhondt (1998) proposed an automatic cutting procedure for finite element modeling of 3-D mode I crack growth. This methodology allows the finite element method to be applied to arbitrarily meshed structures with 20-node elements. During the crack propagation, new 20-node brick elements are automatically generated and a subsequent smoothing procedure improves the quality of the resulting mesh.

Modeling 3-D crack growth encompasses all aspects of the modeling process from initial data preparation to visualization of results. To model an evolving crack efficiently and automatically in a complex 3-D structure, one requires two integral components in a simulator: crack representation and crack growth mechanics. Representation includes the details of storing the geometry of a cracked body in a computer and updating the geometric description to reflect crack growth; this includes both the real geometry and the mathematical representation, i.e. the mesh. Mechanics includes stress analysis, extraction of relevant crack growth parameters, and determination of the shape, extent, and direction of crack growth. These two components form the basis for modeling crack evolution (see Carter 2000 for detail).

In recent years, with the evolution of numerical techniques, there has been an increasing rate of development of simulation codes for fracture analysis such as EPIC (Lim 1996), FRANC3D (Riddell 1997), WARP3D (Koppenhoefer 1998), and so on. The current investigation concentrates on the implementation of crack growth models in the large-scale nonlinear explicit finite element simulation code DYNA3D (Whirley, 1993). The DYNA3D code is used for analyzing the dynamic response of three-dimensional solids and structures. This code uses element removal techniques to simulate the failure process. The crack opening profile therefore can not be modeled. Furthermore, the stress based failure methodology is not able to describe failure characteristics accurately. Therefore, it is important to implement fracture theories for

solving crack propagation problems. The code is most suitable and some specific features of DYNA3D have great advantages for dynamic fracture simulations. A 2-D fracture model was implemented in DYNA3D for a shell element by Marzougui (1998). CTOA and plastic energy criteria were utilized for prediction of crack growth. His work has demonstrated the feasibility of implementing fracture models in DYNA3D. However, further work is still required for the proper implementation of the fracture models for shell elements. The present work concentrates on implementing crack growth models for solid elements in DYNA3D.

METHODOLOGY OF IMPLEMENTING PSEUDO 3-D FRACTURE MODELS IN DYNA3D

In this study, fracture models have been implemented in the DYNA3D code for 3-D crack growth simulations. The implemented fracture models have the capabilities of simulating automatic crack propagation without user intervention. The implementation is carried on solid elements. The input phase subroutines of the DYNA3D code have been modified to read the crack input parameters and allocate memory for the fracture model arrays. A uniform crack growth with prediction of growth direction is implemented. Crack extension can be provoked by several different fracture parameters as follows:

1. The stress intensity factors (K_I, K_{II} and K_{III})
2. Energy release rates (G_I, G_{II} *and* G_{III}) and
3. Crack tip opening angle (*CTOA*).

The maximum circumferential stress criterion is utilized to predict the growth direction. An element-stress based failure methodology is also provided. Similar to the conventional smeared crack approaches, the critical fracture tensile stress is used for activation of crack growth. The crack opening profile, however, is simulated here explicitly. The crack propagates in the direction perpendicular to the maximum principal stress. The implemented procedure can be used to simulate through thickness crack growth. The methodology of implementing the 3-D fracture models is described in the following sections.

Evaluation of Fracture Parameters

In the finite element models for the nonlinear code DYNA3D, an actual 3-D crack shape is modeled with the edges and surfaces of solid elements. To evaluate the fracture characteristics, in this study, the representation of the 3-D crack tip has been decomposed into a series of "*sub-cracks*" at the crack front (see the solid lines in Figure 1). Each sub-crack is defined by three nodes with the identification numbers 1, 2 and 3. For through thickness crack, the fracture parameters are thus taken as the average of the results obtained from all the sub-cracks it encompasses. The evaluated fracture parameters in the developed procedure include the stress intensity factors (K_I, K_{II}, and K_{III}), energy release rates (G_I, G_{II}, *and* G_{III}), and crack tip opening angle (*CTOA*). In the following they are described with some details:

1. Stress intensity factors (K_I, K_{II}, and K_{III})

In this study, the stress intensity factors (SIFs) of the three fracture modes (see Figure 2) are extracted at discrete nodes from the elastic solution (Aliabadi, 1993) of a cracked geometry:

In an elastic crack vicinity, the actual displacements (u_n, u_b, *and* u_t) in the directions normal, binormal and tangent to the crack front (local Cartesian coordinate system, see Figure 3) can be expressed in terms of the polar coordinates r and θ (in the **n**-**b** plane) as

$$u_n = \frac{1+\nu}{4E}\sqrt{\frac{2r}{\pi}}\left\{K_I\left[(2\kappa-1)\cos\frac{1}{2}\theta-\cos\frac{3}{2}\theta\right]+K_{II}\left[(2\kappa+3)\sin\frac{1}{2}\theta+\sin\frac{3}{2}\theta\right]\right\}$$

$$u_b = \frac{1+\nu}{4E}\sqrt{\frac{2r}{\pi}}\left\{K_I\left[(2\kappa+1)\sin\frac{1}{2}\theta-\sin\frac{3}{2}\theta\right]+K_{II}\left[(2\kappa-3)\cos\frac{1}{2}\theta+\cos\frac{3}{2}\theta\right]\right\} \quad (1)$$

$$u_t = \frac{2(1+\nu)}{E}\sqrt{\frac{2r}{\pi}}K_{III}\sin\frac{1}{2}\theta$$

where E is the Young's modulus; ν is the Poisson's ratio; and κ is the Kolosov constant defined as

$$\kappa = \begin{cases} 3-4\nu, & \text{plane strain} \\ \dfrac{3-\nu}{1+\nu}, & \text{plane stress} \end{cases} \quad (2)$$

The plane strain assumption is employed herein for actual 3-D crack analysis. The plane stress case is also implemented in the code for simulations of crack growth in thin shell materials. Substituting θ with $\pm\pi$ into equation (1), the stress intensity factors can be derived from the crack surface displacements as

$$K_I = \frac{E}{(1+\nu)(1+\kappa)}\sqrt{\frac{\pi}{2r}}(u_{b_{\theta=\pi}} - u_{b_{\theta=-\pi}})$$

$$K_{II} = \frac{E}{(1+\nu)(1+\kappa)}\sqrt{\frac{\pi}{2r}}(u_{n_{\theta=\pi}} - u_{n_{\theta=-\pi}}) \quad (3)$$

$$K_{III} = \frac{E}{4(1+\nu)}\sqrt{\frac{\pi}{2r}}(u_{t_{\theta=\pi}} - u_{t_{\theta=-\pi}})$$

In this study, the stress intensity factors for a sub-crack are evaluated from the displacements of its tail nodes (node 1 and node 3, see Figure 1) which should have the same initial coordinates in the initial original FE model. Taking r as the average of the distances from these two nodes to the tip node 2, we have

$$K_I = \frac{E}{(1+\nu)(1+\kappa)}\sqrt{\frac{\pi}{2r}}(u_{b_{\text{node 3}}} - u_{b_{\text{node 1}}})$$

$$K_{II} = \frac{E}{(1+\nu)(1+\kappa)}\sqrt{\frac{\pi}{2r}}(u_{n_{\text{node 3}}} - u_{n_{\text{node 1}}}) \quad (4)$$

$$K_{III} = \frac{E}{4(1+\nu)}\sqrt{\frac{\pi}{2r}}(u_{t_{\text{node 3}}} - u_{t_{\text{node 1}}})$$

Assume a nodal position in terms of the global coordinates has the projections (x_n, x_b, x_t) on the directions of local system. Eqution (4) can finally be rewritten as

$$K_I = \frac{E}{(1+\nu)(1+\kappa)}\sqrt{\frac{\pi}{2r}}(x_{b_{node\ 3}} - x_{b_{node\ 1}})$$
$$K_{II} = \frac{E}{(1+\nu)(1+\kappa)}\sqrt{\frac{\pi}{2r}}(x_{n_{node\ 3}} - x_{n_{node\ 1}}) \quad (5)$$
$$K_{III} = \frac{E}{4(1+\nu)}\sqrt{\frac{\pi}{2r}}(x_{t_{node\ 3}} - x_{t_{node\ 1}})$$

In the implemented fracture models, the stress intensity factors are evaluated by equation (5). They are calculated and monitored at each time step for further crack growth.

2. Energy release rates (G_I, G_{II}, and G_{III})

The total energy release rate, *G*, is the amount of energy made available at the crack tip for the crack extension process per unit area extension of the crack. The expression is given as (Petit, 1996):

$$G = -\frac{\partial \Pi}{\partial a} = -\frac{\partial (U - W)}{\partial a} \quad (6)$$

where Π is the total potential energy per u7nit thickness; *U* is the strain energy of the structure per unit thickness; *W* is the work of the external tractions per unit thickness, and *a* is the crack length. In the current fracture models, based upon linear elastic fracture mechanics (LEFM), the energy release rates corresponding to the three fracture modes are directly calculated from the stress intensity factors using the following relationships (Parker, 1981):

$$G_I = \frac{1}{E'}K_I^2$$
$$G_{II} = \frac{1}{E'}K_{II}^2 \quad (7)$$
$$G_{III} = \frac{1+\nu}{E}K_{III}^2$$
$$G = G_I + G_{II} + G_{III}$$

with *E* (Young's modulus), *v* (Poisson's ratio), and $E'=E$ (plane stress) or $E'=E/(1-\nu^2)$ (plane strain).

3. Crack tip opening angle (*CTOA*)

The crack tip opening angle (CTOA) is another fracture parameter implemented in the code. The evaluation of this parameter is based on sub-crack angles. In the simulation of uniform crack growth, the actual 3-D crack angle is considered as the average of all the sub-crack angles.

Implementation of The 3-D Crack Growth Criteria

Several crack growth criteria have been implemented in the nonlinear explicite finite element code DYNA3D for activation of 3-D crack growth. These crack growth criteria are described below:

a) Maximum principal stress-based criterion

This criterion is an application of the macroscopic mechanics in fracture analyses. In the implemented procedure, the averaged 3-D stress components are obtained from the elements around the crack front and subsequently the maximum principal stresses are calculated. The

crack is assumed to grow once the maximum principal stress exceeds the material fracture tensile stress. Obviously, this criterion requires very fine mesh in the vicinity of the crack tip to obtain an accurate stress distribution and consequently accurate numerical simulation.

b) CTOA-based crack growth criterion

This fracture criterion is based on the macroscopic levels of deformation and has been widely used in elastic-plastic fracture analyses (Andersson 1973; Shih 1979; Newman 1984; Dawicke 1999; and Gullerud 1999). According to this criterion, the crack is extended if the evaluated CTOA exceeds a critical value.

c) SIFs-based mixed-mode criterion

Cracks are assumed to grow once the following equation for the stress intensity factors is satisfied.

$$\left(\frac{K_I}{K_{Ic}}\right)^{\alpha} + \left(\frac{K_{II}}{K_{IIc}}\right)^{\beta} + \left(\frac{K_{III}}{K_{IIIc}}\right)^{\gamma} = 1 \qquad (8)$$

where K_{Ic}, K_{IIc} and K_{IIIc} denote the individual fracture toughness values of the three fracture modes. The constant parameters α, β and γ should be empirically determined and defined by users. If one takes $\alpha = \beta = 2$ and selects appropriate values of K_{IIIc} and γ to ignore the term of the tearing mode (mode III), equation (8) becomes a well-known fracture criterion first proposed by Wu (1967):

$$\left(\frac{K_I}{K_{Ic}}\right)^{2} + \left(\frac{K_{II}}{K_{IIc}}\right)^{2} = 1 \qquad (9)$$

d) Energy release rates-based mixed-mode criterion

Cracks are assumed to grow once the following equation for the energy release rates is satisfied.

$$\left(\frac{G_I}{G_{Ic}}\right)^{\alpha} + \left(\frac{G_{II}}{G_{IIc}}\right)^{\beta} + \left(\frac{G_{III}}{G_{IIIc}}\right)^{\gamma} = 1 \qquad (10)$$

The critical fracture values are denoted by a subscript *c*. With the input parameters $G_{Ic} = G_{IIc} = G_{IIIc} = G_c$ and $\alpha = \beta = \gamma = 1$, equation (10) can be converted to the total energy release rate based fracture criterion (Irwin, 1957), which is given by the following equation:

$$G = G_I + G_{II} + G_{III} = G_c \qquad (11)$$

where G_c is the critical total energy release rate.

e) SIFs-based maximum circumferential stress criterion

Cracks are assumed to grow once the following equation is satisfied.

$$K_e = \cos\frac{\theta_0}{2}\left(K_{Ieff}\cos^2\frac{\theta_0}{2} - \frac{3}{2}K_{II}\sin\theta_0\right) = K_{Ic} \qquad (12)$$

This maximum circumferential stress criterion (Erdogan, 1963) is initially proposed for two-dimensional mixed mode fracture problems. However, it has been extended to three dimensions (Gerstle, 1986) by combining Mode I and Mode III stress intensity factors into an effective mode I stress intensity factor as follows:

$$K_{Ieff} = K_I + B\left|K_{III}\right| \qquad (13)$$

where B is an empirically determined factor for combination of K_I and K_{III}. And K_e is the final effective stress intensity factor. K_{Ic} is the fracture toughness. And θ_0 is the predicted crack growth angle.

Prediction of The Crack Growth Direction

In the implemented fracture models, the maximum circumferential stress criterion is utilized to predict the direction of crack propagation. The crack propagation angle θ_0 is defined as the angle between the line of crack and the crack growth direction with positive value defined in the anti-clockwise direction. Under mixed mode I and II loading, it can be expressed as (Broek, 1986):

$$\theta_0 = 2\tan^{-1}\left(\frac{K_I}{4K_{II}} - \frac{1}{4}\sqrt{\left(\frac{K_I}{K_{II}}\right)^2 + 8}\right) \quad \text{for } K_{II} > 0$$
$$\theta_0 = 2\tan^{-1}\left(\frac{K_I}{4K_{II}} + \frac{1}{4}\sqrt{\left(\frac{K_I}{K_{II}}\right)^2 + 8}\right) \quad \text{for } K_{II} < 0 \tag{14}$$

Combining K_I and K_{III} as in equation (13), the prediction of the crack propagation angle is extended to a 3-D case as follows:

$$\theta_0 = 2\tan^{-1}\left(\frac{K_{Ieff}}{4K_{II}} - \frac{1}{4}\sqrt{\left(\frac{K_{Ieff}}{K_{II}}\right)^2 + 8}\right) \quad \text{for } K_{II} > 0$$
$$\theta_0 = 2\tan^{-1}\left(\frac{K_{Ieff}}{4K_{II}} + \frac{1}{4}\sqrt{\left(\frac{K_{Ieff}}{K_{II}}\right)^2 + 8}\right) \quad \text{for } K_{II} < 0 \tag{15}$$

However, equation (15) is not well suited for numerical calculation since an overflow may occur if K_{II} is close to zero. For an automatic crack growth simulation, a more general formula is desirable to account for all possible loading situations. Mi (1996) has devised a different expression of equation (15) as follows and is used in the current study for prediction of crack growth direction:

$$\theta_0 = 2\tan^{-1}\left(\frac{-2K_{II}}{K_{Ieff} + \sqrt{(K_{Ieff})^2 + 8(K_{II})^2}}\right) \tag{16}$$

The above formula takes the different signs of equation (15) into account and is, from a numerical point of view, a much better expression than equation (15).

Automatic Remeshing Strategy

To model the crack growth explicitly, some modifications have to be carried out on the mesh to update the free crack surfaces and crack tip geometry. Thus additional nodes and elements become necessary. In the DYNA3D code all the data arrays are static (the array sizes are fixed through the simulation), the total number of nodes and elements in the model has to remain constant through the simulation. This introduces a problem in the remeshing strategy: *how to add the new nodes and elements?* Currently this problem has been solved by adding dummy nodes and elements to the initial FE model before the start of simulation.

In the DYNA3D code a failure flag has been provided for each element. Once a failure flag is activated, the corresponding element will be removed from the numerical calculation although it still exists in the data arrays. The element with activated failure flag is also invisible to the post-processors like LS-TAURUS. In this study, the databases of the simulation results are modified to be compatible with LS-TAURUS for visualization of explicit crack opening profile. In the original FE model, initially fictitious coordinates are given to the dummy nodes and failure flags are activated for all the dummy elements. The proposed automatic remeshing strategy models the explicit crack growth by splitting sub-crack tip nodes. When a crack advances, each related crack tip node is assigned with one of the dummy nodes. This dummy node is given the same coordinates and velocities as the sub-crack tip node. The sub-crack tip node shares with the dummy node the original nodal mass. Meanwhile, the element connectivity is updated such that the elements on one side of new crack extension are connected to the added dummy node and the elements on the other side are connected to the original node. Actually the elements connecting the dummy node are the dummy elements newly added. The original elements at that location is deleted by activating their failure flags. The added dummy elements are updated with the same material properties, stresses and strains as the elements they replaced. The status of these dummy elements is changed by invalidating their failure flags. For compatibility with LS-TAURUS, the D3PLOT result file is also modified such that the used dummy nodes have the same initial coordinates as the corresponding sub-crack tip nodes and the elements have the current element connectivity.

To better understand the automatic remeshing strategy, a 2-D finite element mesh is utilized here for illustration (see Figure 4). Figure 4a depicts a previous mesh before crack extension. Assume that the current predicted crack direction vector lies in the element *A*, whose vertexes are identified with the numbers 1, 2, 3 and 4. Three different remeshing patterns are possible herein as follows:

- Pattern 1: *Node number 2 is the nearest vertex to the predicted crack direction vector.*
  In this case, node *2* is moved along the element edge *2-3* to create the current crack growth direction. A dummy node *1'* is then added to the location of node *1*. The elements *A* and *B* in the previous mesh are deleted by activating their failure flags. Accordingly two new dummy elements *A'* and *B'* are activated to replace the elements *A* and *B*. Current elements *A'* and *B'* take the new node *1'* as their vertex and a new crack profile is thus generated (see Figure 4b).

- Pattern 2: *Node number 3 is the nearest vertex to the predicted crack direction vector.*
  After moving node *3* to current crack tip position, a dummy node *1'* is added to the location of node *1*. The previous elements A and B are removed. The unoccupied region is then filled with three new elements *A'*, *A''* and *B'*. The elements *A'* and *B'* are connected to the new node *1'*, and the element *A''* still uses the original node *1* as its vertex (see Figure 4c).

- Pattern 3: *Node number 4 is the nearest vertex to the predicted crack direction vector.*
  Here, node *4* is moved along the element edge *3-4* to create the direction of current crack propagation. After introducing the new node *1'*, only element *B* in the previous mesh is required to be removed. The new element B' is then added with the vertex of node *1'*. (see Figure 4d).

As stated above, the presented fracture models generate the direction of crack propagation by moving previous mesh nodes along the element edges. When a crack reaches free edges (or surfaces) of structures, some nodes on the free edges might be required to move. This creates minor geometric change, which is observed in the local crack tip regions at the free edge. However, this effect is insignificant to fracture analyses since it only occurs in the last step of crack growth.

VALIDATION OF THE PSEUDO 3-D FRACTURE MODELS

In this section, seven crack problems are used to verify the proposed fracture models. All finite element meshes are modeled with solid elements. The maximum circumferential stress criterion is employed to determine the crack growth direction. Different mesh sizes or loading rates are utilized in some examples in order to study the effect of these parameters on the behavior and characteristic of crack propagation. The numerical simulations are validated quantitatively and qualitatively. All the crack growth processes are automatically simulated without user intervention. LS-TAURUS is employed as the post-processor to visualize explicit crack opening profiles. The seven crack propagation examples considered are presented next with some details.

1. Static stress intensity factor of a central horizontal crack in a square plate

Stress intensity factors (SIFs) play an important role on the current implementation of the fracture procedure. It is necessary to investigate the accuracy of SIFs evaluated by the displacement method. Figure 5 describes a benchmark problem to study the effect of mesh sensitivity (Xie, 1995). The model is a square plate with a horizontal central crack subjected to remotely applied uniform vertical traction σ = 1.0 MPa. The geometry, material properties and boundary conditions are shown in Figure 5. The exact value for the stress intensity factor K_I is 4.72 MPa(m)$^{1/2}$ (Tada, 1973). Figure 6 shows a typical mesh used here for the study of mesh sensitivity where the mesh has the same number of elements, *n* for the rows and columns and five layers through the thickness. In an explicit FE program like DYNA3D the evaluated SIFs are always given as a function of time. To obtain the "static" K_I, in this example the traction is applied as a ramp load first and then kept constant after 1.0 second for total of 2.0 seconds simulation (see Figure 7). It is well accepted that explicit dynamic codes with long duration simulation are an acceptable way of simulating quasi-static problems. Table 1 shows the results (at 2.0 second) of the computed K_I from the different meshes considered.

Table 1. Simulated results for a central horizontal crack plate
(exact solution: K_I = 4.72 MPa(m)$^{1/2}$)

Number of Elements	K_I, MPa(m)$^{1/2}$ (at 2.0 second)
8×8×5	2.33
16×16×5	3.74
24×24×5	4.28
40×40×5	4.74

Good correlation occurs in the mesh of 40×40×5 elements. The comparison indicates that the SIFs could be underestimated by coarse meshes. Therefore, appropriate element size should be selected by users to get acceptable accuracy.

2. Dynamic stress intensity factors of a central inclined crack in a finite plate

This example deals with the determination of dynamic stress intensity factors of 3-D cracks. The crack is inclined at 45° in a finite rectangular plate as shown in Figure 8. The plate is loaded dynamically in the axial direction by a tensile traction σ = 400 MPa (step function in time). The plain strain solution was first presented by Chen and Wilkins (1976) using finite differences and has been frequently used as a reference to validate other methods such as the quarter-point FEM (Murti, 1986b), time domain BEM (Dominguez, 1992) and EFG method (Krysl, 1999).
In this example, the problem is studied using 3-D solid elements (the thickness of the plate being set to 10 mm, 5 layers of elements through the thickness). Two typical meshes are used herein for validation. Figure 9 shows the top views of the meshes (2976 elements in coarse mesh and 10144 elements in fine mesh). The material is linear elastic with properties as reported by Chen and Wilkins (1976): E = 200000 MPa, ν = 0.3 and ρ = 5000 kg/m^3. Figure 10 shows mode-I and mode-II stress intensity factors versus time respectively normalized by $\sigma(\pi a)^{1/2}$. For validation the figures also depict the more recent numerical results reported by Dominguez & Gallege (1992) and Krysl & Belytschko (1999). It can be seen that the present results from both meshes are in good agreement with the reference solutions. However, the coarse mesh causes slight underestimation of the peak values.

3. Load-crack extension curve of Al 2024-T3 M(T) specimens

Gullerud et al. (1999) presented the load-crack extension experimental data from five 2024-T3 M(T) aluminum specimens tested at NASA-Langley. The specimens were 75 mm in width and 2.3 mm through thickness. The central horizontal crack is 25 mm long. The experiment consisted of applying a tensile load incrementally and measuring the load versus crack extension. A system of guide plates was employed to minimize the out-of-plane deformation during the tension.

Figure 11 shows the FE model (7500 elements and two layers through the thickness) used herein. The length (L_0) of the plate is twice as much as the width. The remote tensile load is applied by displacement control. Opposite constant velocities (V) are imposed on both ends of the plate. The material properties of 2024-T3 aluminum alloy used here is provided by Dawicke and Newman (1999): an elastic modulus of 71400 MPa and a yield stress of 345 MPa. A piece-wise linear representation of the tensile stress-strain curve is given in Table 2. The CTOA criterion is employed to predict the crack growth. The critical CTOA value is taken as 5.25° (Dawicke, 1999). In this example, the load-crack extension curve is predicted by the proposed fracture model and compared with experimental results (see Figure 12).

Table 2. Tensile stress-strain curve for 2.3 mm thick 2024-T3 aluminum alloy

Strain	0.00483	0.015	0.04	0.1	0.16	0.2
Stress, MPa	345	390	430	470	490	490

Different loading rates are considered in this example to investigate the convergence and the sensitivity to the loading rate (V/L_0). The static stress-strain relationship is used here although it should be justified in a dynamic analysis. Figure 13 shows the analytic results of remote applied stress versus the crack extension at the loading rates (V/L_0) of 1.0, 0.5, 0.25, 0.025 and 0.0025 s^{-1} respectively. The results indicate that a greater peak value of the curve occurs at a higher loading rate. The convergence of the analytic results can be observed at 0.25, 0.025 and 0.0025 s^{-1}. These three convergent curves are also depicted in Figure 12 to compare with the quasi-static test data.

The proposed fracture model provides an acceptable prediction, which is in good agreement with the test results.

4. Mixed-mode fracture of a central horizontal crack in a square plate

This example was used by Marzougui (1998) to validate his fracture model. It is a square plate with a central horizontal crack (see Figure 14). The plate is subjected to mixed-mode loading which is applied by superposing a normal stress σ_y (mode I) and a shear stress τ_{xy} (mode II). The ratio of the normal and shear stresses is dependent on the normal stress factor *s* and the shear stress factor *t*. Eight cases with different stress ratios are considered in this example (see Table 3). Figure 15 shows the FE model (4800 elements, 3 elements through the thickness) with the linear elastic properties: E = 210000 MPa, ν = 0.28. The CTOA criterion is employed to activate crack advancement. The critical value is taken as 0.19.

For an infinite plate with central crack under mixed-mode loading as shown in Figure 14, the stress intensity factors (K_I and K_{II}) can be expressed in terms of the normal and shear stresses as follows (Broek, 1986):

$$\begin{aligned} K_I &= \sigma_y \sqrt{\pi a} = s\sigma\sqrt{\pi a} \\ K_{II} &= -\tau_{xy}\sqrt{\pi a} = -t\sigma\sqrt{\pi a} \end{aligned} \qquad (17)$$

Substituting K_I and K_{II} into equation (14) leads to the crack growth angle θ_0 prediction equation as follows:

$$\theta_0 = 2\tan^{-1}\left(-\frac{s}{4t} + \frac{1}{4}\sqrt{\left(\frac{s}{t}\right)^2 + 8}\right) \qquad (18)$$

Equation (18) is used here to compute the theoretical crack growth with the different ratios (*s*/*t*) of stress factors. The theoretical and simulated results are listed in Table 3 for comparison.

Table 3. Crack growth angle under mixed-mode loading

Case	s	t	θ_0 (Theoretical)	θ_0 (Simulated)
1	1.0	0.1	11.203°	11.375°
2	1.0	0.2	21.089°	21.401°
3	1.0	0.3	29.103°	29.623°
4	1.0	0.4	35.357°	35.898°
5	1.0	0.5	40.208°	40.607°
6	1.0	0.6	44.004°	44.243°
7	1.0	0.7	47.022°	47.918°
8	1.0	0.8	49.460°	49.068°

It can be concluded that the current implementation of the fracture model can predict the mix-mode crack growth direction very well.

5. Dynamic crack propagation simulation of interacting cracks

This is an interesting example for dynamic crack propagation simulation. The problem involves two interacting edge cracks in a sheet. The cracks at two sides of the sheet are slightly misaligned to provide initial asymmetry. During the crack propagation three stages can be detected: initially the cracks repel from each other, as growth continues, they attract. The final intersection of the two cracks results in the ejection of a small elliptical piece of material. This

crack interaction phenomenon was experimentally observed by Sinha et al. (1986). Numerical simulations were also reported in the literature (Swenson 1987; Liebowitz 1995; and Marzougui 1998).

To verify the effectiveness of current implementation of the fracture model, the dynamic propagation processes of two interacting cracks is simulated. The FE model (6480 elements and two layers through the thickness) is shown in Figure 16. Initially the two edge cracks are slightly inclined to provide asymmetry. A constant velocity is imposed on both ends of the plate for tension. The material properties of 2024-T3 aluminum alloy are employed for the simulation. The crack growth is controlled by the CTOA criterion. Figures 17 and 18 show the close-up views of the finite element mesh at different stages of crack propagation. At each crack growth step the geometry of the plate is automatically remeshed to generate new explicit crack opening profiles. The sequential growth steps are automatically determined by numerical solutions without user intervention. This example can be considered a rather severe test of current fracture model. As shown in Figures 17 and 18, current fracture model effectively captures the interaction of the two cracks: initial avoidance, later attraction and final separation.

6. Crack path deflection due to a hole

This example was used by Rashid (1998) to simulate the response of an evolving edge crack when approaching a circular hole. The example considers a cracked rectangular plate containing an off-center circular hole (see Figure 19). Uniform normal traction is loaded along the top and bottom edges of the plate. In such a non-self-similar crack growth problem, the effect of the hole's presence is plainly evident in the crack path. The crack deflection is very dependent on initial crack location. An initial location close to the hole could cause the crack path to intersect the hole, whereas the crack path is more nearly straight for initial locations that are more remote from the hole.

In this example three different initial locations of the crack are considered. Figure 19 depicts the initial FE models (2688 elements and two layers through the thickness) and final deformed meshes as well as 3-D shaded geometry. The material properties of 2024-T3 aluminum alloy and the CTOA crack growth criterion are used in this example. The plots illustrate that the automatic-remeshing fracture model can reasonably represent the individual crack deflection corresponding to different initial crack locations.

7. Growth of cracks emanating from circular holes

Figure 20 shows a square plate with cracks emanating from two small holes subjected to far-field tensile loading. In the initial configuration, both cracks have a length of 0.2 in and are oriented at 45° and -45° for the left and right holes, respectively. This problem was presented by Belytschko et al. (1995) to validate the development of the Element-Free Galerkin method for crack propagation simulation. This example is utilized here to test the current fracture model. Mesh sensitivity and loading rate effects are also studied here.

In this example, constant velocities V are loaded at the remote edges of the plate to create tension. The thickness of the plate is set to 0.06 in and two layers of solid elements are modeled. For all the nodes in the model proper constraints are applied to simulate plain strain conditions. Figure 21 shows the top view of a coarse mesh (2976 elements) used herein. A refined mesh (10144 elements) and a more refined mesh (56200 elements) are also considered in the study. Close-up views of theses three different meshes are depicted in Figure 22. To investigate the

loading rate effects, the rates (V/L_0) of 50.0, 5.0, 0.5 and 0.05 s^{-1} are considered in the simulations respectively. This study uses the linear elastic properties of AISI 4340 steel (Sih, 1984): $E = 30\times10^6$ psi, $\nu = 0.3$ and $K_{Ic} = 43.0$ ksi $(in)^{1/2}$ (plain strain). The effective SIF based fracture criterion, equation (12), is employed in this example. The same value of K_{Ic} is utilized in all the cases although actual fracture toughness should vary with loading rate.

Figure 23 provides the simulation results at the rate of 50.0 s^{-1} with 3-D shaded geometry (the scale factor of displacement is set to 10 for better visualization). The crack path curves from the different meshes with the different loading rates are plotted to clarify the comparison (see Figures 24 and 25). At the rate of 0.05 s^{-1} no simulation is performed for the finest mesh since it required much computation time (this loading rate required millions of cycles in the explicit finite element simulation). The simulations indicate that the cracks eventually grow towards the holes. More discrepancy of the crack paths occurs at a higher loading rate (50.0 s^{-1}). At the rate of 5.0, 0.5 or 0.05 s^{-1}, very good correlation can be observed among the coarse and fine meshes. Although, slight divergence of the crack paths can be detected at the area close to the hole. The computations in this area are undoubtedly prone to error, since the stress intensity factors changes rapidly as the crack approaches the free surface (Belytschko, 1995). In this example, for either coarse or fine mesh, the simulated crack path is little sensitive to the low loading rates. Theoretically the antisymmetry of geometry and mesh pattern will lead to two antisymmetric crack path curves. The growth of each crack should be identical at each step. However, current fracture model gives an unexpected prediction for the finest mesh at the loading rate of 0.5 s^{-1}. The antisymmetry of the crack growth is disturbed as the cracks approach the holes. The left crack grows into the right hole sooner than the right crack and consequently no further growth occurs on the right crack. This phenomenon might be triggered by numerical roundoff errors.

DISCUSSION AND CONCLUSIONS

Modeling of 3-D explicit crack growth processes has rarely been attempted in finite element simulations that utilizes solid elements. This is because of the difficulty in updating the geometric description to reflect the evolving crack propagation. In the presented work the implementation of 3-D crack growth models in the large-scale nonlinear explicit finite element simulation code DYNA3D is conferred. The first stage of the work is presented in this paper, which consists on the implementation of a pseudo 3-D fracture models. An automatic remeshing strategy is described herein. Explicit crack opening profiles are modeled by splitting crack tip nodes. An element deletion and replacement procedure is proposed and presented. The failure flag provided in the code is used for each element to control its absence or involvement in numerical calculations. Elements with activated failure flag are invisible to the post-processors like LS-TAURUS and crack tip geometry is thus displayed explicitly. The use of failure flags makes it possible to implement fracture procedure in this code. The proposed methodology has the capabilities of modeling automated 3-D through thickness crack growth processes.

Fracture parameters such as stress intensity factors, energy release rates and crack tip opening angle are evaluated. The direction of crack propagation is determined from the maximum circumferential stress criterion. Currently this option only can be used for simulation of through thickness crack growth. The implemented fracture models have been validated through several crack problems. Mesh sensitivity and loading rate effects are studied in the presented examples. Simulations indicate that the proposed methodology is capable in predicting

a curved crack path automatically and efficiently even though the crack growth direction is unknown a priori. However, it is found that the stress intensity factors could be underestimated in a coarse element mesh. To gain acceptable accuracy, appropriate element size has to be selected by users. The development of DYNA3D code with the 3-D fracture procedure is still in the progress. Significant effort is concentrated on improvement of current methodology and implementation of more theoretical or numerical algorithms. The further work will be presented at a later time.

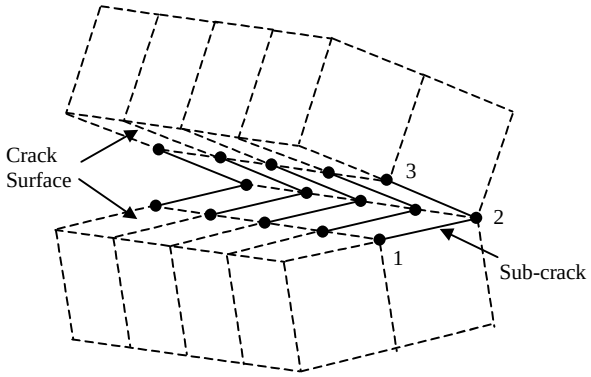

Figure 1. Decomposition of a 3-D crack tip.

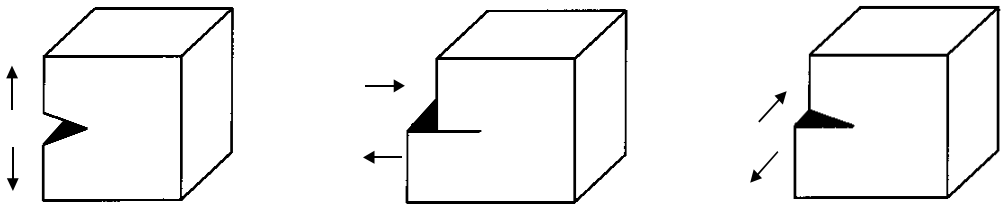

(a) Mode I (*opening mode*) (b) Mode II (*shearing mode*) (c) Mode III (*tearing mode*)

Figure 2. Three modes of fracture

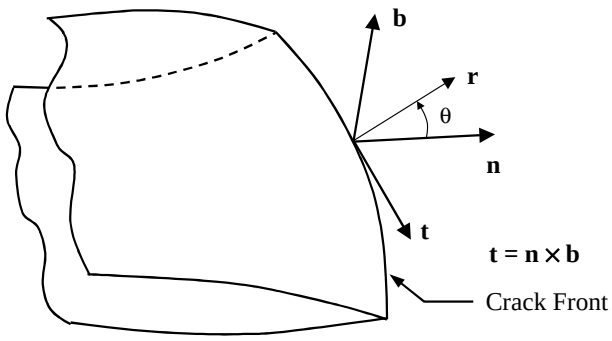

Figure 3. Local coordinates at a 3-D crack front

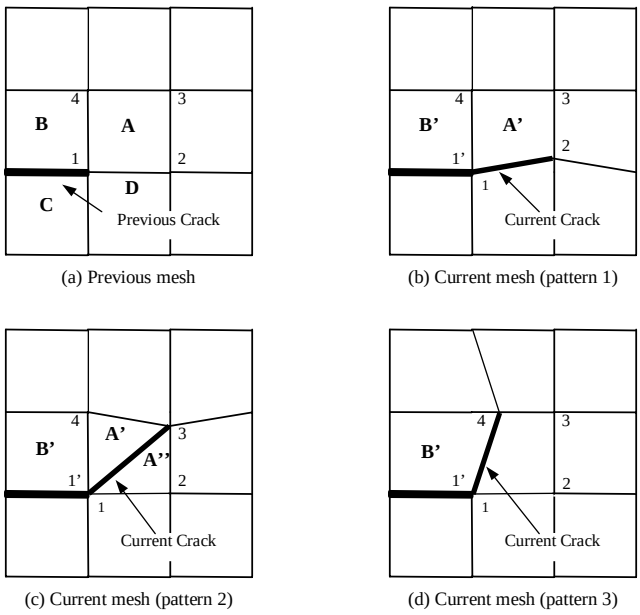

Figure 4. Automatic remeshing strategy for crack propagation

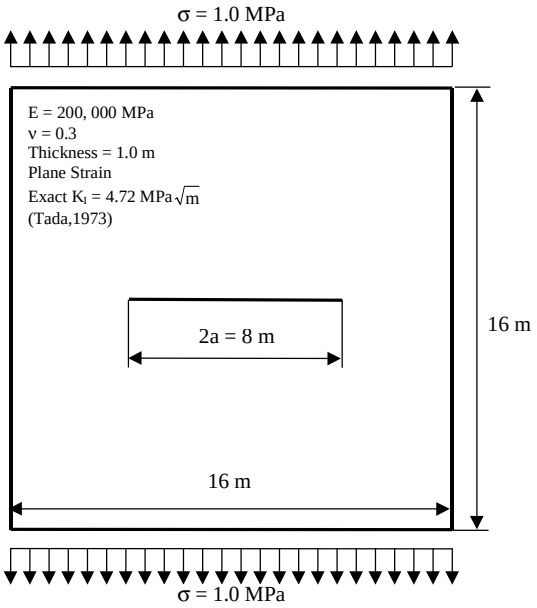

Figure 5. Statement of central horizontal crack problem

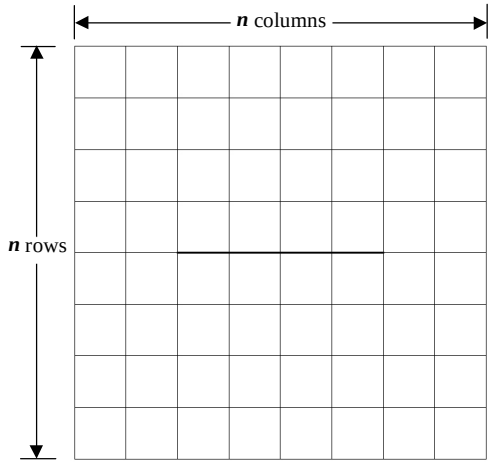

Figure 6. FE model of central crack plate

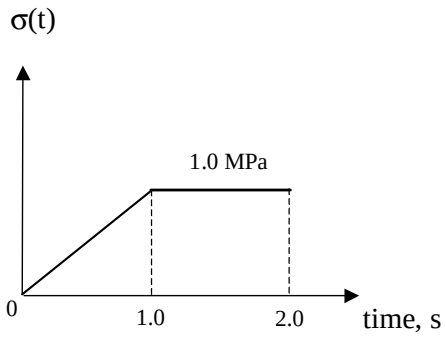

Figure 7. Load curve of remote traction

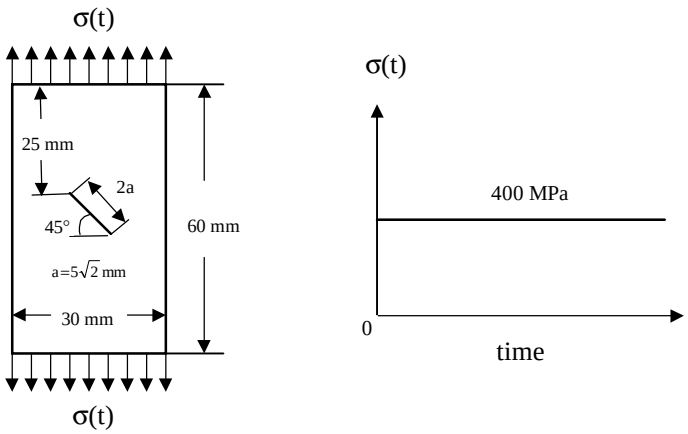

Figure 8. Plate with a central inclined crack under a uniform step tensile load

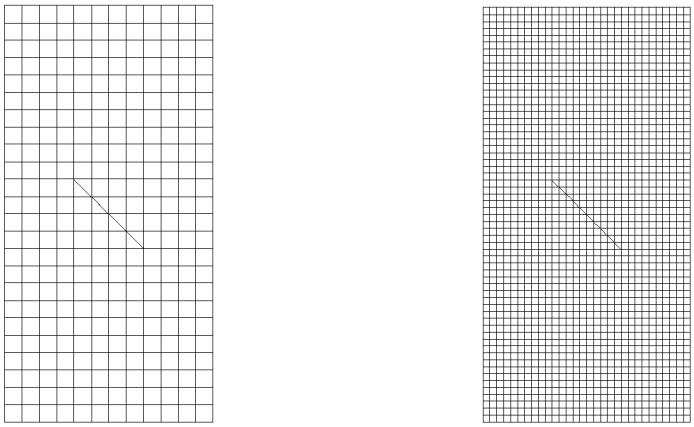

(a) Coarse mesh (b) Fine mesh

Fingure 9. FE model for plate with a central inclined crack

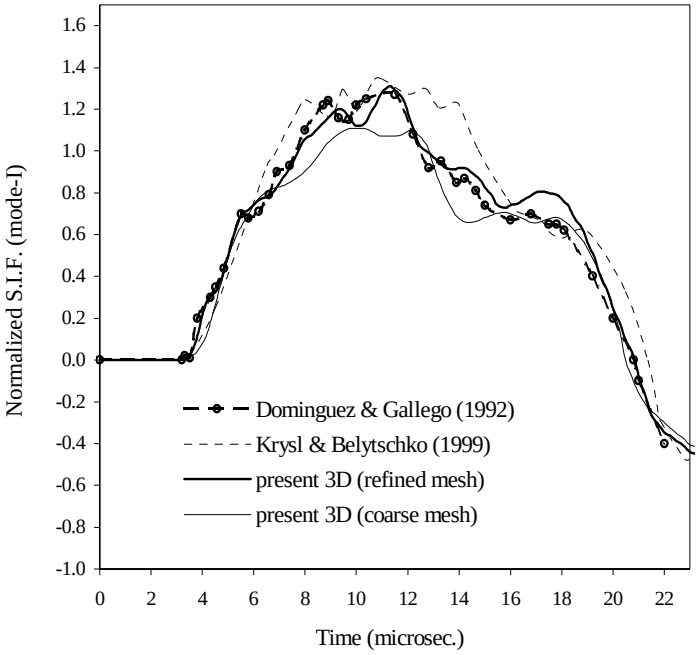

(a) Normalized mode-I SIF versus time

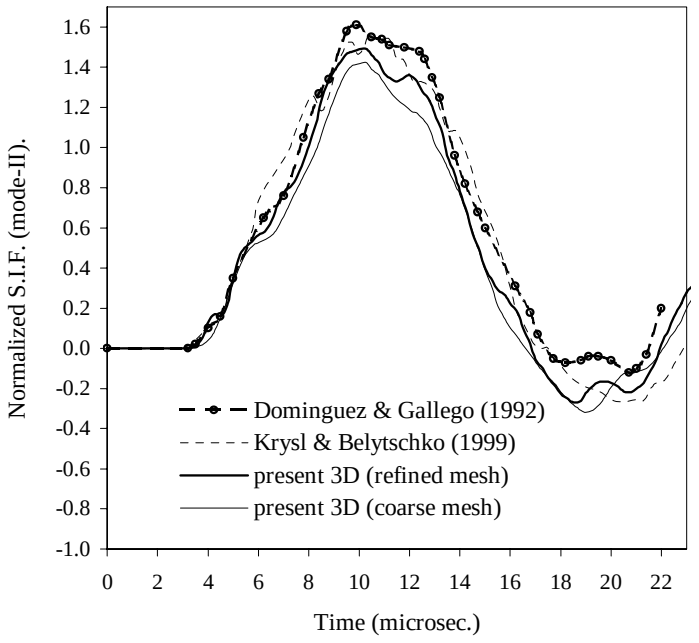

(b) Normalized mode-II SIF versus time

Figure 10. Dynamic stress-intensity factors of a central inclined crack in a finite plate

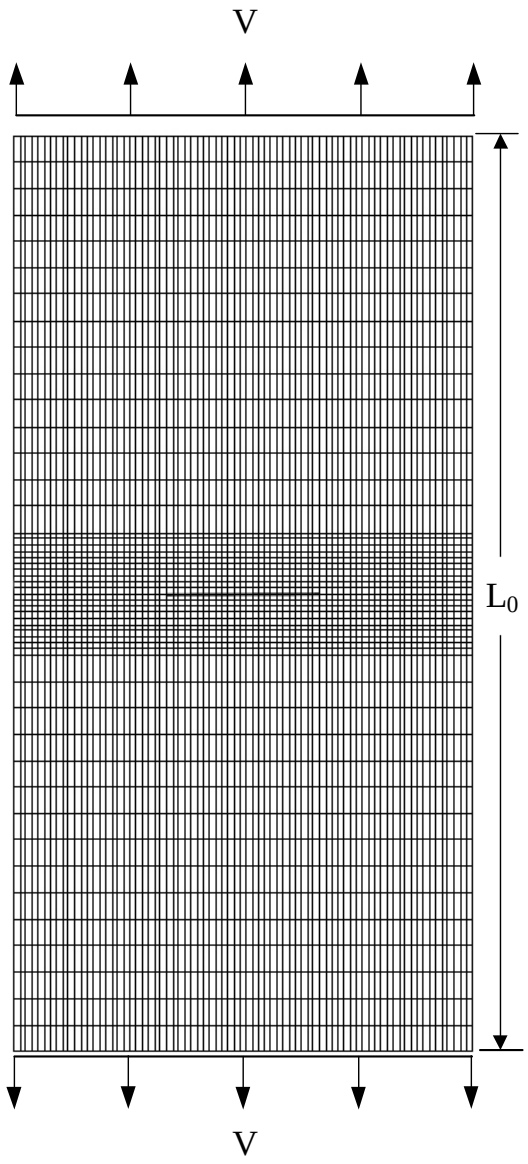

Figure 11. FE model for extnsion of an Al 2024-T3 M(T) specimen

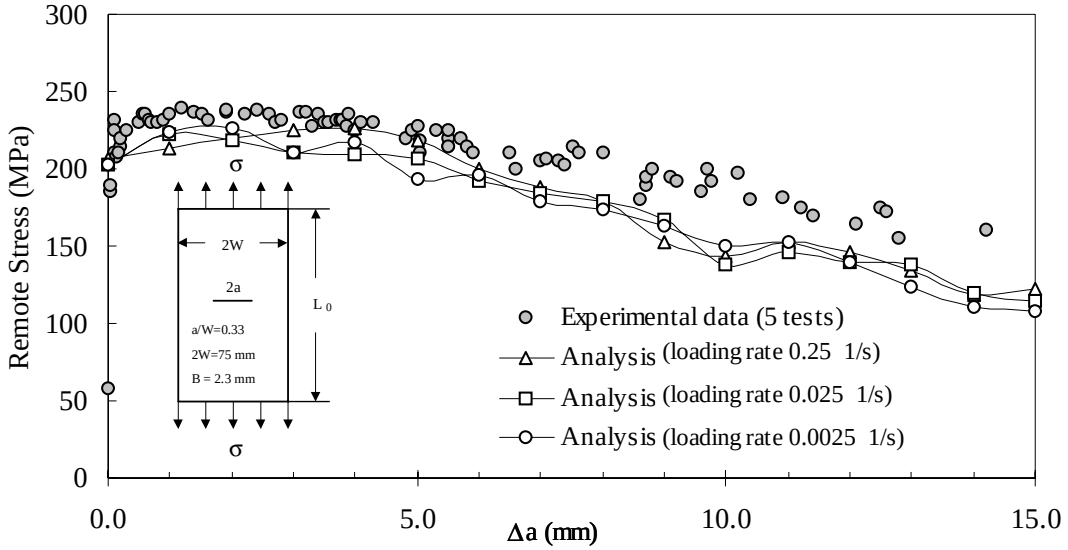

Figure 12. Comparison of experimental and analytical load-crack growth response

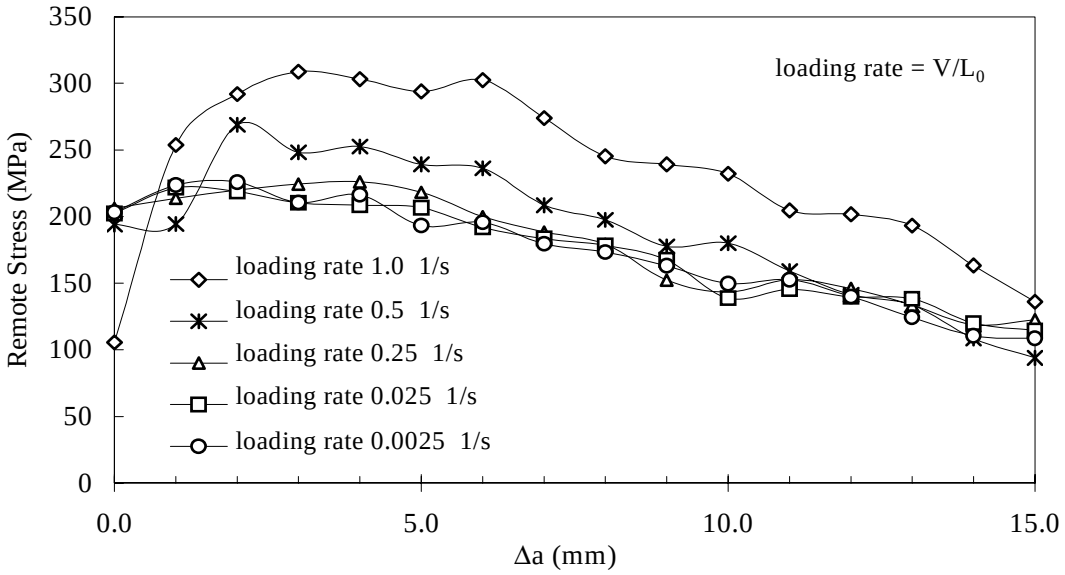

Figure 13. Analytical load-crack growth response at different loading rates

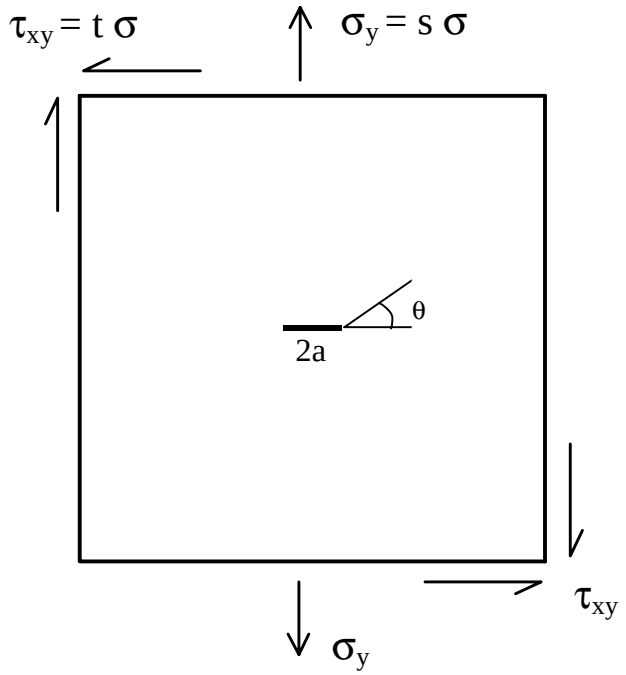

Figure 14. Plate with central horizontal crack under mixed-mode loading

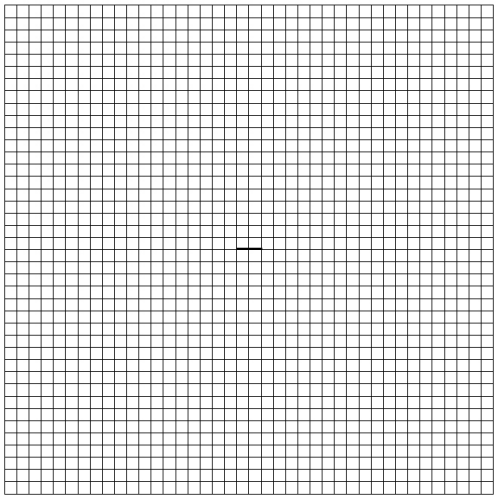

Figure 15. FE model of a plate with central horizontal crack

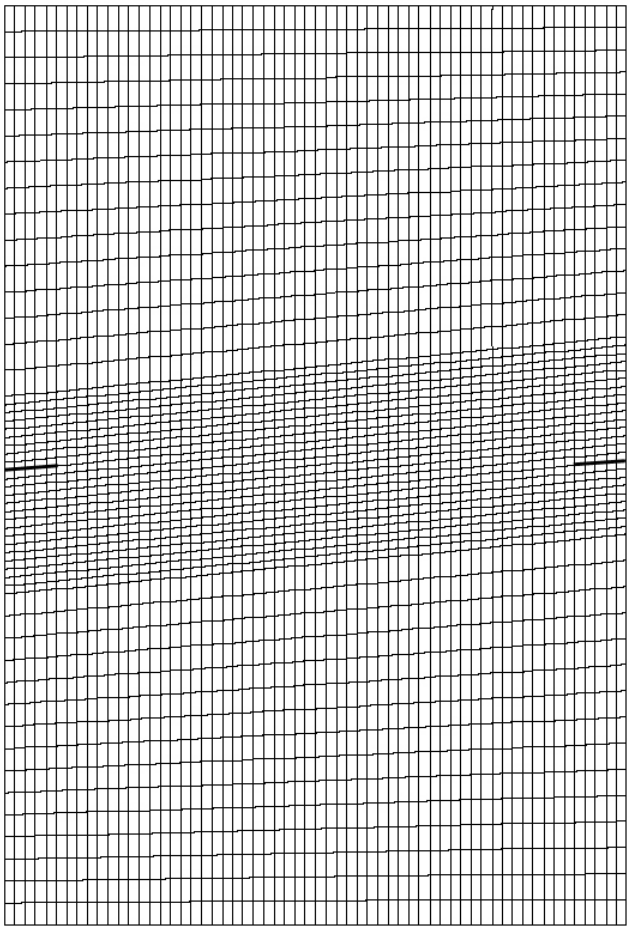

Figure 16. FE model for a finite plate with two asymmetric cracks

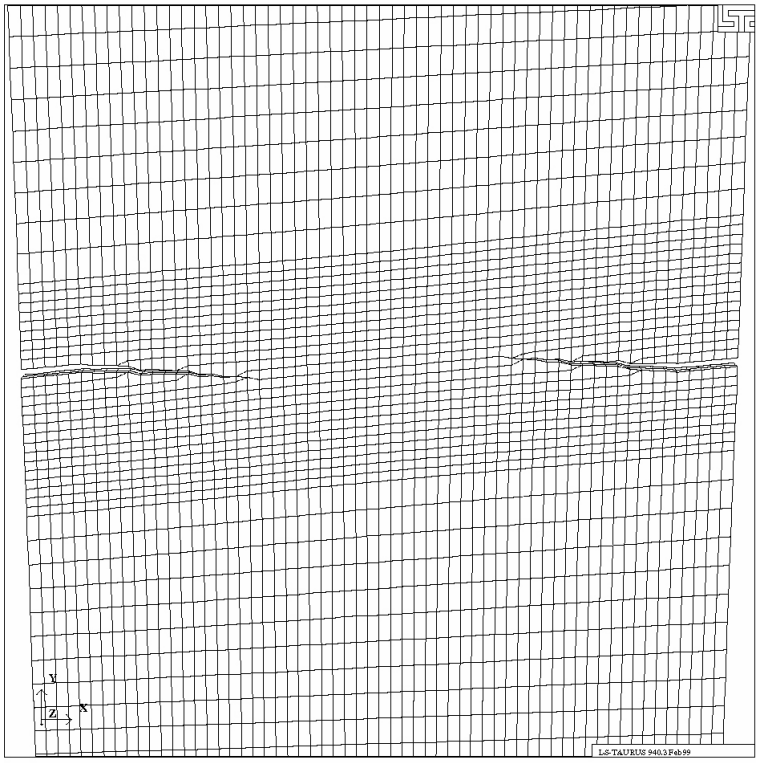

(a) Initial propagation

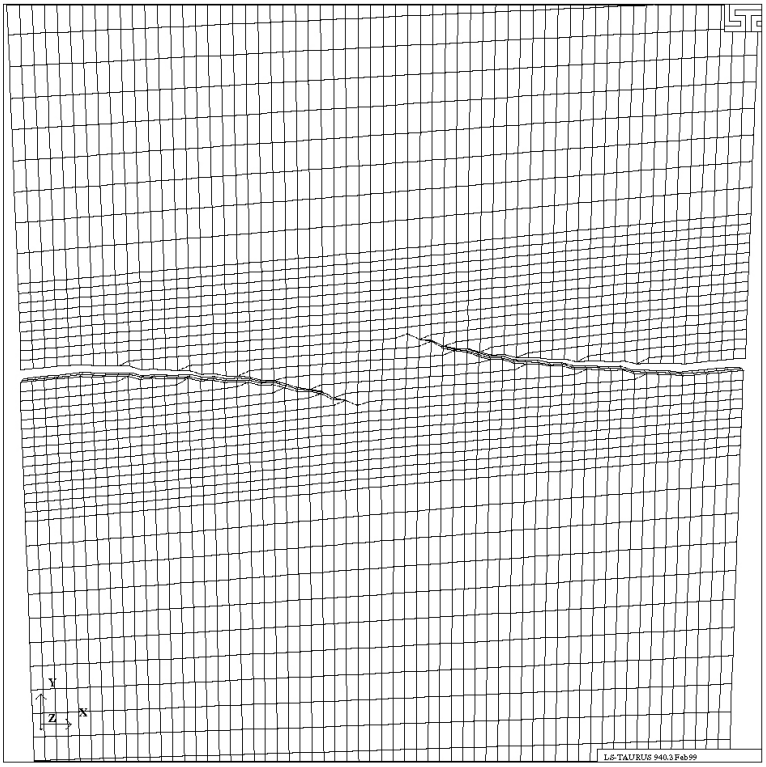

(b) Crack avoidance

Figure 17. Dynamic crack propagation simulation of interacting cracks

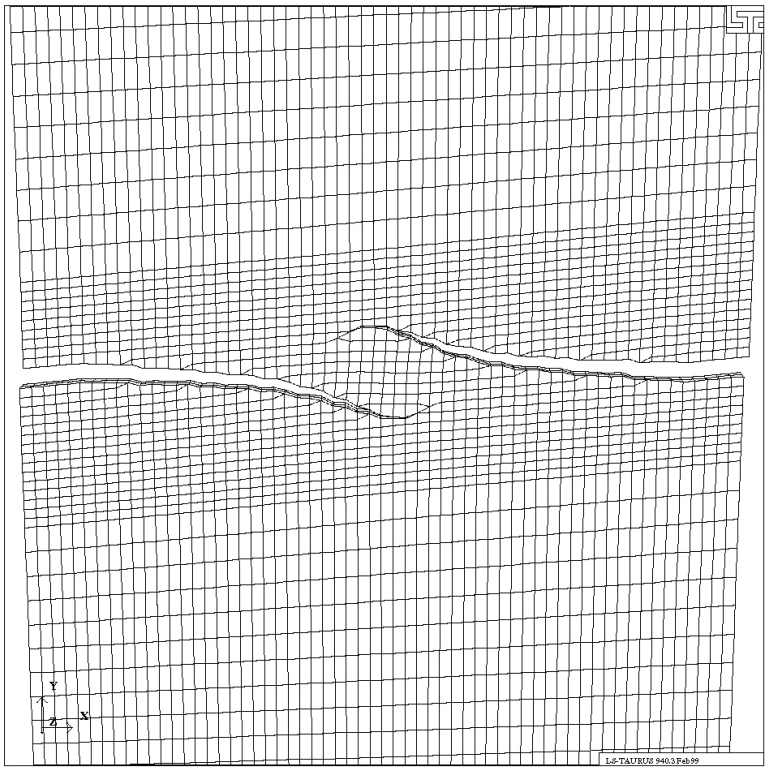

(c) Crack attraction

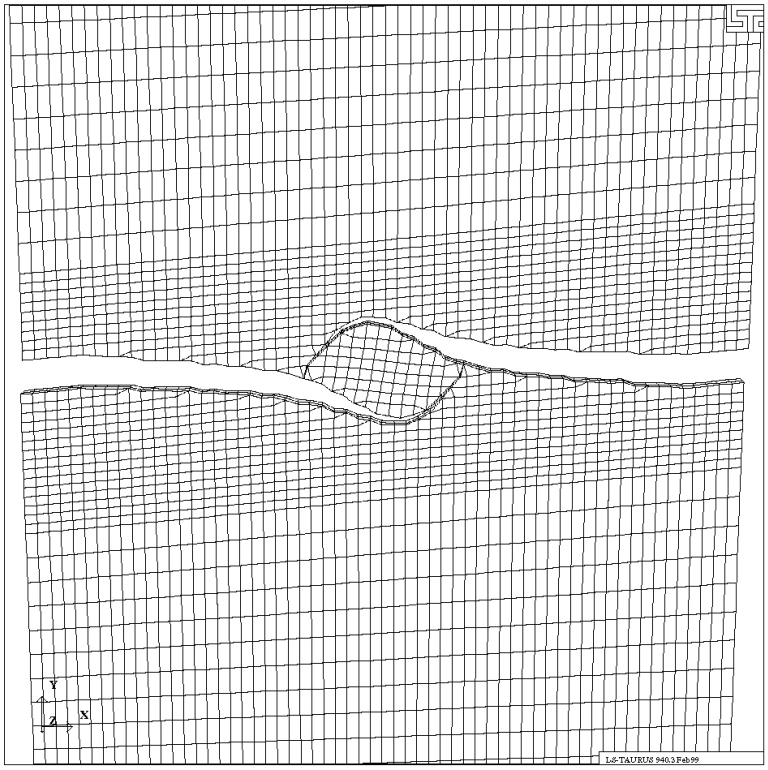

(d) Final separation

Figure 18. Dynamic crack propagation simulation of interacting cracks (contined)

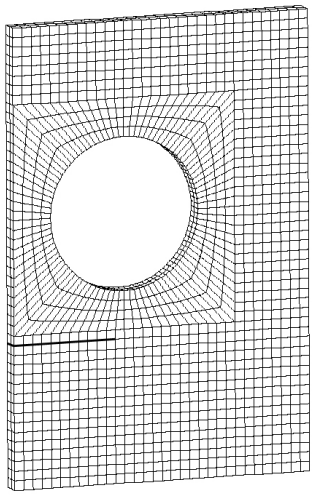

initial geometry (mesh)

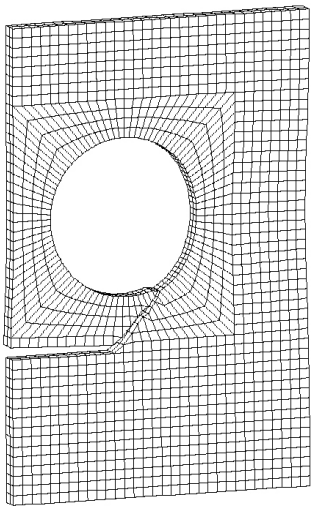

final geometry (mesh)

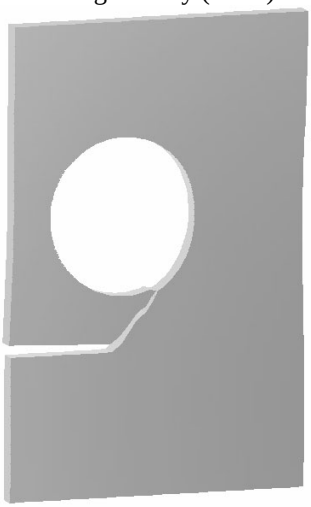

final geometry (shaded)

(a) Initial location of crack is close to the hole

Figure 19. Crack path deflection due to a hole

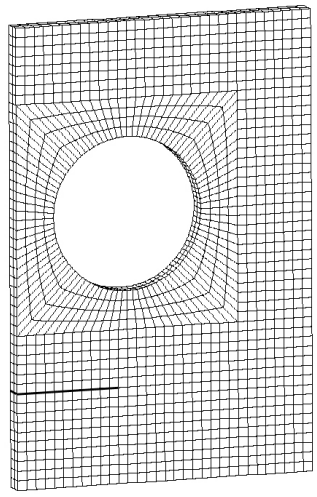

initial geometry (mesh)

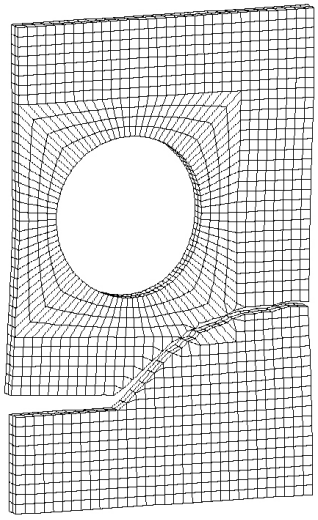

final geometry (mesh)

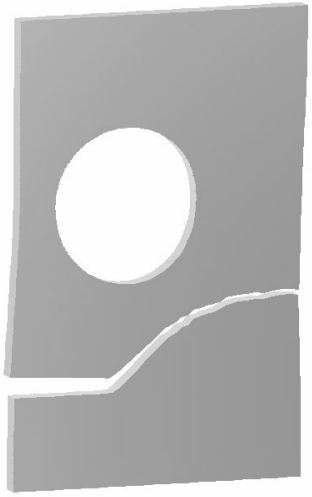

final geometry (shaded)

(b) Initial location of crack is remote to the hole

Figure 19. Crack path deflection due to a hole

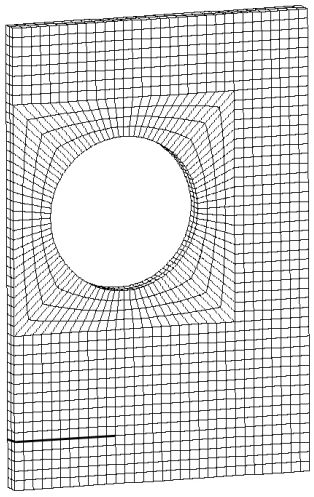

initial geometry (mesh)

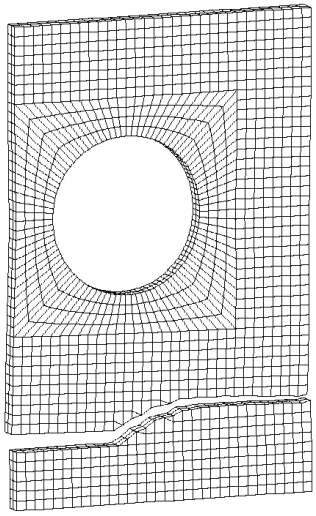

final geometry (mesh)

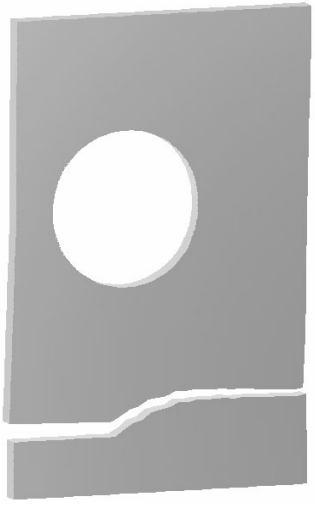

final geometry (shaded)

(c) Initial location of crack is more remote to the hole

Figure 19. Crack path deflection due to a hole

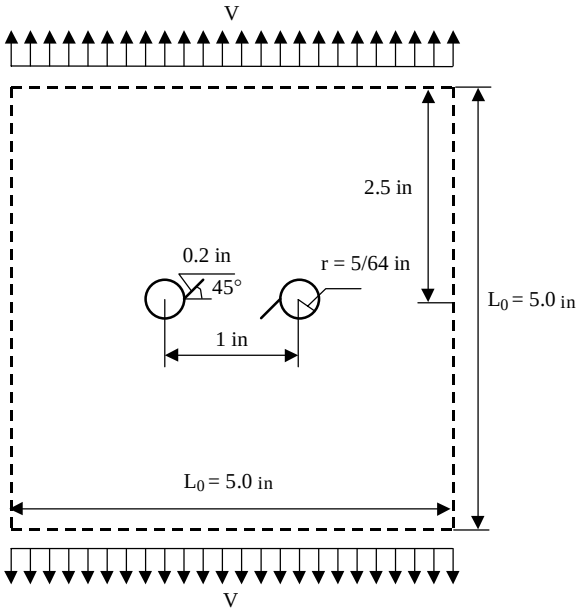

Figure 20. Statement of growth of cracks emanating from circular holes

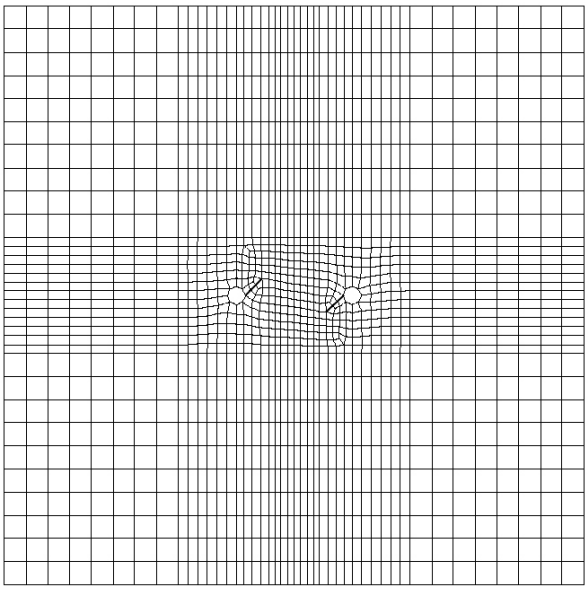

Figure 21. Coarse mesh for a square plate with cracks emanating from two holes

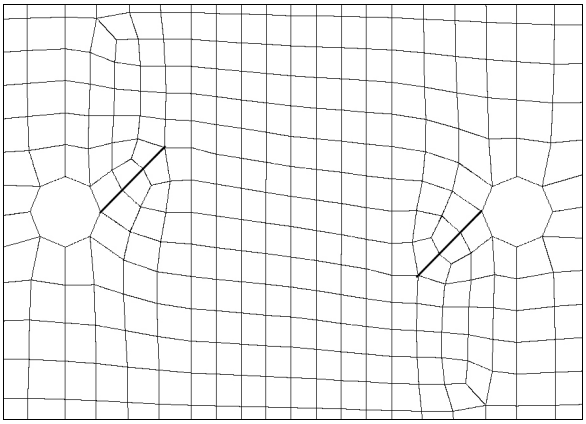

(a) Coarse mesh

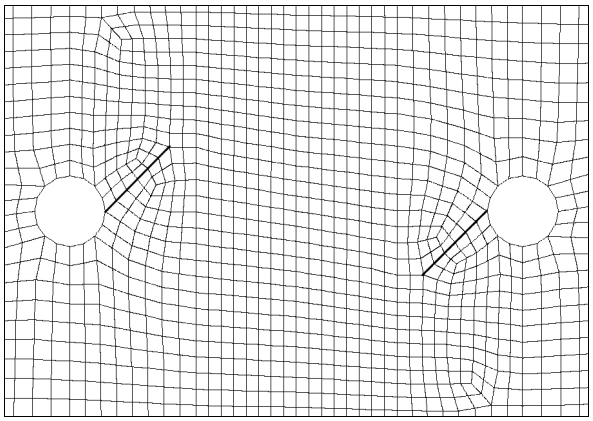

(b) Refined mesh

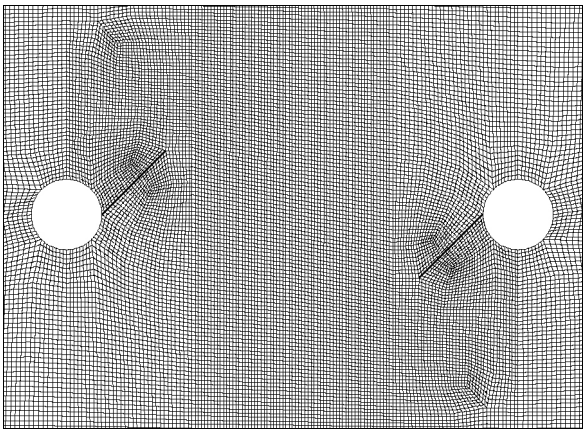

(c) More refined mesh

Figure 22. Close-up views of FE models with different mesh sizes

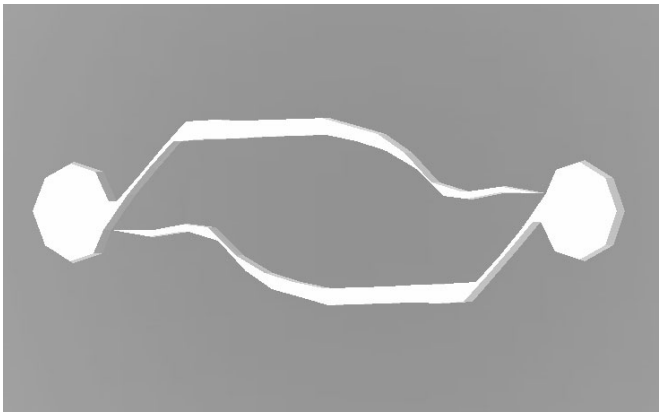

(a) Coarse mesh

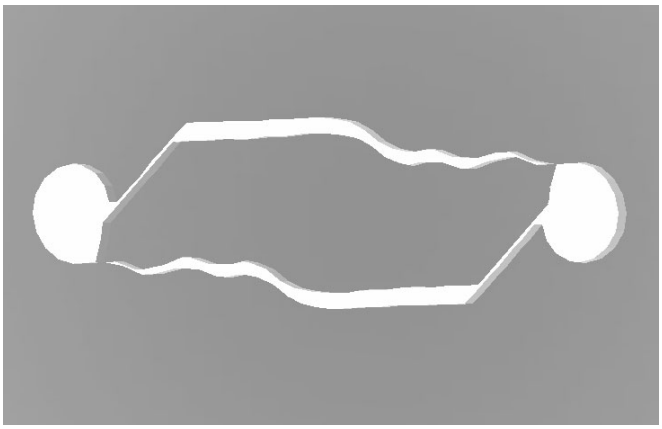

(b) Refined mesh

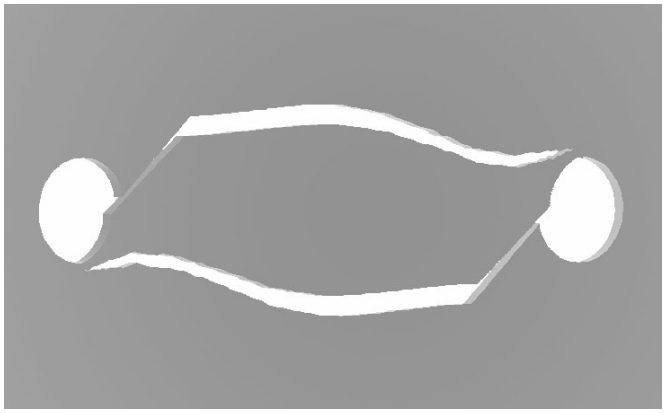

(c) More refined mesh

Figure 23. Simulated results (3-D shaded geometry) at the loading rate of 50.0 s^{-1}
(The scale factor of displacement is set to 10)

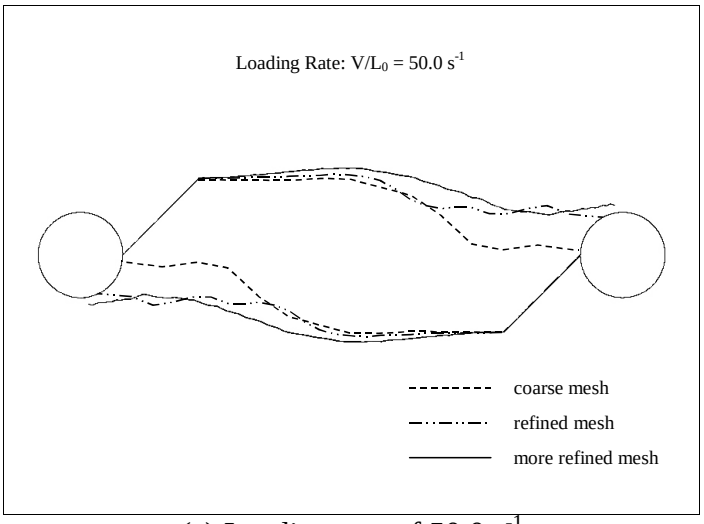

(a) Loading rate of 50.0 s^{-1}

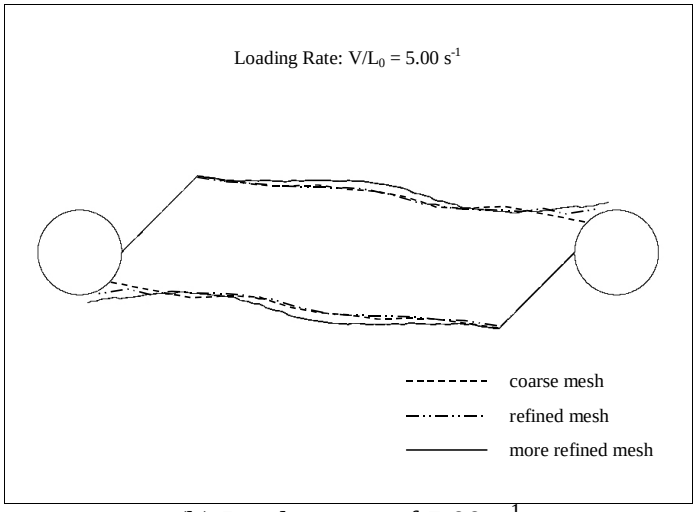

(b) Loading rate of 5.00 s^{-1}

Figure 24. Study of mesh sensitivity and loading rate effects

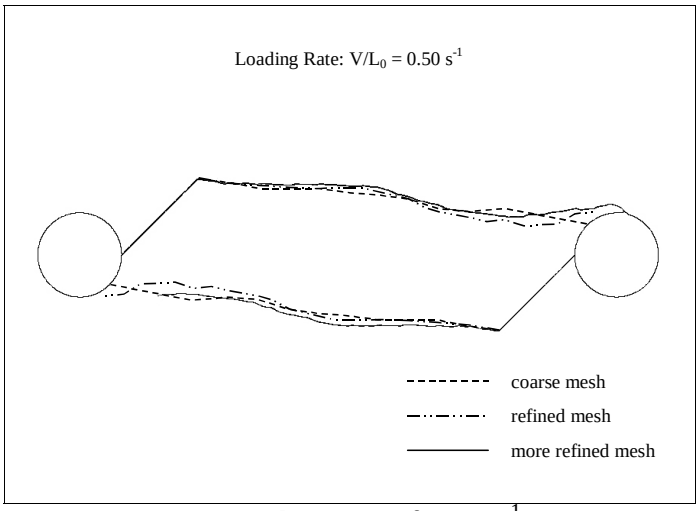

(c) Loading rate of 0.50 s^{-1}

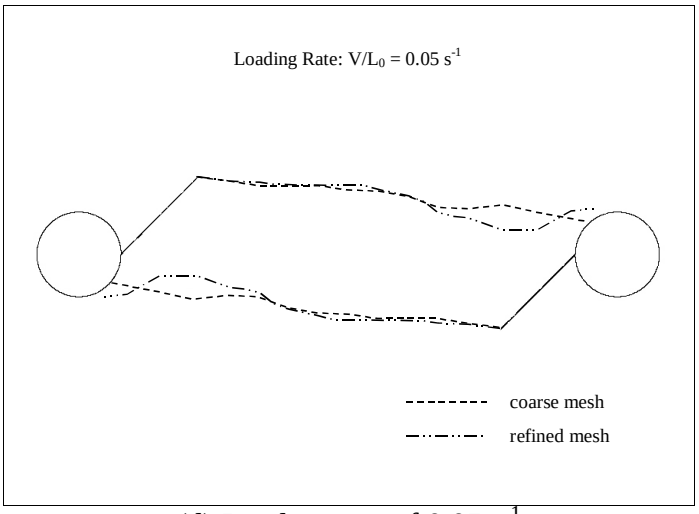

(d) Loading rate of 0.05 s^{-1}

Figure 25. Study of mesh sensitivity and loading rate effects (continued)

ACKNOWLEDGMENTS

The principle author would like to extend sincere thanks to the Lawrence Livermore National Laboratory (LLNL) for providing the source codes for DYNA3D. Computing support was provided by the Ohio Supercomputer Center. Their support is gratefully acknowledged.

REFERENCES

1. Aliabadi, M.H. (1997a). "Boundary element formulations in fracture mechanics." *Applied Mechanics Reviews* 50, pp.83–96.
2. Aliabadi, M. H. (1997b) " A new generation of boundary element methods in fracture mechanics." *Int. J. Fract.*, Vol. 86, pp. 91-125.
3. Aliabadi, M. H., and Brebbia, C. A., eds. (1993). Advances in boundary element methods for fracture mechanics. Computational Mechanics Publications, Southampton, UK.
4. Andersson, H. (1973). "A finite-element representation of stable crack-growth." *J. Mech. Phys. Solid*, Vol. 21, pp. 337-356.
5. Argyris, J. H., Faust, G., and Willam, K. J. (1979). Finite element analysis of concrete cracking. ISD-Report No. 254, Stuttart.
6. Atluri, S. N., and Kathisesan, K. (1980). "Influence of flaw shape on stress intensity factors for pressure vessel surface flaws and nossel corners." *J. Press. Vess. Technol.*, Vol. 102, pp. 278-286.
7. Barsoum, R. S. (1977). "Triangular quarter-point elements as elastic and perfectly-plastic crack tip elements." *Int. J. Numer. Meth. Engng.*, Vol. 11, pp. 85-98.
8. Belytschko, T., Lu, Y. Y., and Gu, L. (1994). "Element-free Galerkin methods." *Int. J. Numer. Meth. Engng.*, Vol. 34, pp. 229-256.
9. Belytschko, T., Lu, Y. Y., and Gu, L. (1995a). "Crack propagation by element-free Galerkin methods." *Engineering Fracture Mechanics*, Vol. 51, pp. 295-315.
10. Belytschko, T., Lu, Y. Y., Gu, L., and Tabbara, M. (1995b). "Element-free Galerkin methods for static and dynamic fracture." *Int. J. Solids Structures* Vol. 32, pp. 2547-2570.
11. Belytschko, T., and Black, T. (1999). "Elastic crack growth in finite elements with minimal remeshing." *Int. J. Numer. Meth. Engng.*, Vol. 45, pp. 601-620.
12. Bolukbasi, A. O., and Laananen, D. H. (1995). "Analytical and experimental studies of crushing behavior in composite laminates." *Journal of Composite Materials*, Vol. 29, pp. 1117-1139.
13. Broek, D. (1986). Elementary Engineering Fracture Mechanics, Martinus Nijhoff Publishers, Dordrecht, The Netherlands.
14. Carter, B. J., Wawrzynek, P. A., and Ingraffea, A. R. (2000). "Automated 3-D crack growth simulation." *Int. J. Numer. Meth. Engng.*, Vol. 47, pp. 229-253.
15. Chang, F. K., and Chang, K. Y. (1987). "A progressive damage model for laminated composites containing stress concentrations." *Journal of Composite Materials*, Vol. 21, pp. 834-855.
16. Chen, Y. M., and Wilkins, M. L. (1976). "Stress analysis of crack problems with a three dimensional time dependent computer program." *Int. J. Fract.*, Vol. 12, pp. 607-617.
17. Dawicke, D. S., and Newman, J. C., Jr. (1999). "Residual strength predictions for multiple site damage cracking using a three-dimensional finite element analysis and a CTOA criterion." *Fatigue and Fracture Mechanics*, Vol. 29, ASTM STP 1332, pp. 815-829.

18. Dhondt, G. (1998a). "Automatic 3-D model I crack propagation calculations with finite elements." *Int. J. Numer. Meth. Engng.*, Vol. 41, pp. 739-757.
19. Dhondt, G. (1998b). "Cutting of a 3-D fiite element mesh for automatic mode I crack propagation calculations." *Int. J. Numer. Meth. Engng.*, Vol. 42, pp. 749-772.
20. Dominguez, J., and Gallego, R. (1992). "Time domain boundary element method for dynamic stress intensity factor computations." *Int. J. Numer. Meth. Engng.*, Vol. 33, pp. 635-647.
21. Erdogan, F., and Sih, G. C. (1963). "On the crack extension in plates under plane loading and transverse shear." *Journal of Basic Engineering, Transition of ASME*, Vol. 85, pp. 519-527.
22. Gerstle, W. H. (1986). Finite and boundary element modelling of crack propagation in two- and three-dimensions using interactive computer graphics, Ph.D. thesis, Cornell University, Ithaca, NY.
23. Gullerud, A. S., Dodds, R. H., Hampton, R. W., and Dawicke, D. S. (1999). "Three-dimensional modeling of ductile crack growth in thin sheet metals: computational aspects and validation." *Engineering Fracture Mechanics*, Vol. 63, pp. 347-374.
24. Henshell, R. D., and Shaw, K. G. (1975). "Crack tip finite element are unnecessary." *Int. J. Numer. Meth. Engng.*, Vol. 9, pp. 495-507.
25. Hwang, W. C. and Sun, C. T. (1989). "Failure analysis of laminated composites by using iterative three-dimensional finite element method." *Computers & Structures*, Vol. 33, pp. 41-47.
26. Irwin, G. R. (1957). "Analysis of stresses and strains near the end of a crack traversing a plate." *Trans ASME, J. Appl. Mech.*, Vol. 24, pp. 361-364.
27. Keegtra, P. N. R., Head, J. L., and Turner, C. E. (1978). "A two-dimensional fracture dynamic linear-elastic finite-element program for the analysis of unstable crack propagation and arrest." in: A. R. Luxmoore and D. R. J. Owen, eds., Numerical Methods in Fracture Mechanics (University College, Swansea), pp. 634-647.
28. Koenke, C., Harte, R., Kratzig, W. B., and Rosenstein, O. (1998). "On adaptive remeshing techniques for crack simulation problems." *Engineering Computations*, Vol. 15, pp. 74-88.
29. Koppenhoefer, K. C., Gullerud, A. S., Ruggieri, C., Dodds, R. H., Jr., and Healy, B. E. (1998). WARP3D User's Guide – Release 11.0, Structural Research Series No. 607, Department of Civil Engineering, University of Illinois at Urbana-Champaign, Urbana, IL.
30. Krysl, P., and Belytschko, T. (1999). "The element free galerkin method for dynamic propagation of arbitrary 3-D cracks." *Int. J. Numer. Meth. Engng.*, Vol. 44, pp. 767-800.
31. Lee, C. K., and Lo, S. H. (1992). "An automatic adaptive refinement finite element procedure for 2D elastostatic analysis." *Int. J. Numer. Meth. Engng.*, Vol. 35, pp. 2189-2210.
32. Lee, J. D. (1982). "Three dimensional finite element analysis of damage accumulation in composite laminate." *Computers & Structures*, Vol. 15, pp. 335-350.
33. Liebowitz, H., and Moyer, E. T., Jr. (1989). "Finite element methods in fracture mechanics." *Computers & Structures*, Vol. 31, pp. 1-9.
34. Liebowitz, H., Sandhu, J. S., Lee, J. D., and Menandro F. C. M. (1995). "Computational fracture mechanics: research and application." *Engineering Fracture Mechanics*, Vol. 50, pp. 653-670.
35. Lim, I. L., Johnston, I. W., and Choi, S. K. (1996). " A finite element code for fracture propagation analysis within elasto-plastic continuum." *Engineering Fracture Mechanics*, Vol. 53, pp. 193-211.
36. Marzougui, Dhafer (1998). Implementation of a fracture failure model to a 3d nonlinear dynamic finite element code (DYNA3D). Ph.D. Thesis, The George Washington University, VA.

37. Mi, Y., and Aliabadi, M. H. (1994). "Three-dimensional crack growth simulation using BEM." *Comput. Struct.*, Vol. 52, pp. 871-878.
38. Mi, Y. (1996). Three-dimensional analysis of crack growth, Topics in Engineering Vol. 28 (C. A. Brebbia and J. J. Connor, eds.), Computational Mechanics Publications, Ashurst Lodge, Ashurst, Southampton, UK.
39. Murti, V., and Valliappan, S. (1986). "The use of quarter point element in dynamic crack analysis." *Engineering Fracture Mechanics*, Vol. 23, pp. 585-614.
40. Newman, J. C., Jr. (1984). "An elastic-plastic finite element analysis of crack initiation, stable crack growth, and instability." in: Stanford R. J., editor, Fracture Mechanics: fifteenth symposium, ASTM STP 833, Philadelphia: American Society for Testing and Materials, pp. 93-117.
41. Parker, A. P. (1981). The mechanics of fracture and fatigue. E. & F. N. Spon Ltd, London.
42. Petit, C., Vergne, A., and Zhang, X. (1996). "A comparative numerical review of cracked materials." *Engineering Fracture Mechanics*, Vol. 54, pp. 423-439.
43. Portela, A. (1993). Dual boundary element analysis of crack growth, Topics in Engineering Vol. 14 (C. A. Brebbia and J. J. Connor, eds.), Computational Mechanics Publications, Ashurst Lodge, Ashurst, Southampton, UK.
44. Rankin, C. C., Brogan, F. A., and Riks, E. (1993). "Some computational tools for the analysis of thrpugh cracks in stiffened fuselage shells." *Comput. Mech.*, Vol. 13, pp. 143-156.
45. Rashid M. M. (1998). "The arbitrary local mesh replacement method: an alternative to remeshing for crack propagation analysis." *Comput. Methods Appl. Mech. Engng.* Vol. 154, pp. 133-150.
46. Riddell, W. T., Ingraffea, A. R., and Wawrzynek, P. A. (1997). "Experimrntal observations and numerical predictions of three-dimensional fatigue crack propagation." *Engineering Fracture Mechanics*, Vol. 58, pp. 293-310.
47. Scordelis, A. C. (1972). "Finite element analysis of reinforced concrete structures." *Proc. of the Specialty Conference on Finite Element Method in Civil Engineering*, Montreal, Quebec, Canada, pp. 71-114.
48. Shih, C. F., deLorenzi, H. G., and Andrews, W. R. (1979). "Studies on crack initiation and stable crack growth." in: Landes J. D., Begley J. A., Clarke G. A., eds., Elastic-plastic Mechanics, ASTM STP 668, Philadelphia: American Society for Testing and Materials, pp. 65-120.
49. Sih, G. C., and Faria, L., eds. (1984). Fracture mechanics methodology. Martinus Nijhoff Publishers, The Hague, The Netherlands.
50. Sinha, K. R. Y., Fourney, W. L., Baker, D. B., and Dick, R. D. (1986). "Dynamic photoelastic investigation of two pressurized cracks approaching one another." *Engineering Fracture Mechanics*, Vol. 23, pp. 237-249.
51. Swenson, D., and Ingraffea A. (1987). "A finite element model of dynamic propagation with an application to intersecting cracks." in: A. R. Luxmore, et al., eds., Numerical Methods in Fracture Mechanics, Pineridge Press, Swansea, U.K., pp. 191-204.
52. Tada, H., Paris, P., and Irwin, G. (1973). The stress analysis of cracks handbook. Del Res. Corp., Hellertown, Penn.
53. Vaziri, R., Olson, M. D., and Anderson, D. L. (1992). "Finite element analysis of fibrous composite structures: a plasticity approach." *Computers & Structures*, Vol. 44, pp. 103-116.
54. Wawrzynek, P. A., and Ingraffea, A. R. (1991). Discrete modeling of crack propagation. Theoretical Aspects and Implementation Issues in Two and Three Dimensions, Department of Structural Engineering, Report Number 91-5, Cornell University, Ithaca, NY.

55. Whirley, R. G., and Engelmann, B. E. (1993). DYNA3D user manual, Lawrence Livermore National Laboratory.
56. Wu, E. M. (1967), "Application of fracture mechanics to anisotropic plates." *Trans ASME, J. Appl. Mech.*, Vol. 34, pp. 967-974.
57. Xie, M., Gerstle, W. H., and Rahulkumar, P. (1995). "Energy-based automatic mixed-mode crack-propagation modeling." *Journal of Engineering Mechanics*, Vol. 121, pp. 914-923.
58. Yagawa, G., Sakai, Y., and Ando, Y. (1977). "Analysis of a rapidly propagating crack using finite elements." in: G. T. Hahn and M. F. Kanninen, eds., Fast Fracture and Crack Arrest, ASTM STP 627, pp. 109-122.